

EFFECTIVE IMPLEMENTATION OF THE
MICROBLOWING TECHNIQUE ON AIRFOILS

BY

AIDEAL CZAR ZOHARY

A thesis submitted in fulfilment of the requirement for the
degree of Master of Science (Mechanical Engineering)

Kulliyyah of Engineering
International Islamic University Malaysia

MAY 2021

ABSTRACT


The Micro Blowing Technique (MBT) which has been proven by NASA to reduce skin friction drag on a flat plate by up to 70 to 80 percent in the subsonic speed regime, outperforms the conventional blowing by means of adopting micro holes to ensure the introduction of minimal effective roughness. Past researchers have failed to effectively apply MBT on airfoils. The aim of this study is to ensure reduction in both components of drag on an airfoil in subsonic flows through investigating proper selection of airfoils and strategic blowing placement. Based on a detailed in-depth analysis of their work and reasons for earlier failures, a conclusion has been reached that MBT performs well on concave pressure-recovery type of airfoils when positioned in the positive pressure drag region on the lower surface near the trailing edge. The S1223 airfoil that has a sufficient extent of this region while featuring high-lift properties and mild stall characteristics makes it an excellent candidate for effective MBT applications and UAV design. Demonstrated evidence through numerical investigation showed that a proper implementation of MBT on a S1223 airfoil improves its lift-to drag ratio by 30%. A simple and effective CFD modelling of MBT on a Clark Y airfoil shows trends similar to published experimental data involving hot wire and wake pressure measurements. Results consist of the effect of Reynolds number, blowing fraction and contribution of individual drag components to aid understanding on how MBT influences the overall flow and drag. The CFD results are also validated against XFOIL. The findings indicate that total drag reduction is heavily dependent in the manner in which MBT affects the pressure distribution around the airfoil. A proper selection of the region in which micro blowing is located will lead to a significant reduction in pressure drag. At a Reynolds number of 0.3×10^6 , drop in skin friction drag reached almost 5% while reduction in pressure drag is about 37.5% across a range of angles of attack when having MBT applied at 0.68-0.80 x/c. It is concluded that the integration of properly located MBT on concave pressure-recovery type of airfoils should produce significant improvement in their performance.

ملخص البحث

تقنية النفخ الدقيق (MBT) التي أثبتتها وكالة ناسا لتقليل مقاومة الاحتكاك السطحي على لوحة مسطحة بنسبة تصل من 70 إلى 80 بالمائة في عند سرعة دون سرعة الصوت ، تتفوق على النفخ التقليدي من خلال اعتماد ثقب دقيقة لضمان الحد من خشونة السطح. فشل الباحثون السابقون في تطبيق MBT بفعالية على الجنيحات. ومع ذلك ، بناءً على تحليل تفصيلي متعمق لعملهم و في أسباب الفشل السابق ، توصلنا إلى إستنتاج مفاده أن MBT تؤدي أداءً جيداً في نوع الجنيحات المقعرة لاستعادة الضغط عند وضعها في منطقة سحب الضغط الإيجابي على السطح السفلي بالقرب من نهاية الحافة الخلفية. الجنيح S1223 الذي يتمتع بمساحة كافية من هذه المنطقة مع خصائص الرفع العالي وخصائص زاوية انهيار خفيفة يجعله مرشحاً ممتازاً لتطبيقات MBT الفعالة وتصميم الطائرات بدون طيار. أظهرت الأدلة التي تم إثباتها من خلال التحقيق العددي أن التنفيذ المناسب لـ MBT على الجنيح S1223 يحسن نسبة الرفع إلى القوة العكسية بنسبة 30%. تُظهر نمذجة CFD البسيطة والفعالة لـ MBT على جناح كلارك Y اتجاهات مشابهة للبيانات التجريبية المنشورة التي تتضمن القياسات باستخدام السلك الساخن و قياس الضغط خلف الجنيح. تتضمن النتائج تأثير رقم رينولدز وجزء النفخ ومساهمة مكونات القوة العكسية الفردية للمساعدة في فهم كيفية تأثير MBT على التدفق العام والقوة العكسية. يتم التحقق من صحة نتائج CFD أيضاً مقابل نتائج XFOIL. تشير النتائج التي توصلنا إليها إلى أن تقليل القوة العكسية الكلي يعتمد بشكل كبير على الطريقة التي تؤثر بها MBT على توزيع الضغط حول الجنيح. سيؤدي التحديد المناسب للمنطقة التي يقع فيها النفخ الدقيق إلى انخفاض كبير في مقاومة الضغط. عند رقم رينولدز 300000 ، وصل الانخفاض في مقاومة الاحتكاك السطحي إلى ما يقرب من 5% بينما يكون تقليل مقاومة الضغط حوالي 37.5% عبر مجموعة من زوايا الهجوم عند تطبيق MBT عند مسافة نسبتها إلى طول الجنيح (x/c) 0.68-0.80. نستنتج أن استخدام MBT بشكل صحيح على نوع الجنيحات المقعرة لاستعادة الضغط يجب أن ينتج عنه تحسن كبير في أدائها.

APPROVAL PAGE

I certify that I have supervised and read this study and that in my opinion, it conforms to acceptable standards of scholarly presentation and is fully adequate, in scope and quality, as a thesis for the degree of Master of Science (Mechanical Engineering)


.....
Waqar Asrar
Supervisor

.....
Erwin Sulaeman
Co-Supervisor

.....
Mohammed Aldheeb
Co-Supervisor

I certify that I have read this study and that in my opinion it conforms to acceptable standards of scholarly presentation and is fully adequate, in scope and quality, as a thesis for the degree of Master of Science (Mechanical Engineering)

.....
Amelda Dianne Andan
Internal Examiner

.....
Andrew Ragai Henry Rigit
External Examiner

This thesis was submitted to the Department of Mechanical Engineering and is accepted as a fulfilment of the requirement for the degree of Master of Science (Mechanical Engineering)

.....
Meftah Hrairi
Head, Department of Mechanical
Engineering

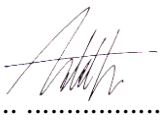
This thesis was submitted to the Kulliyyah of Engineering and is accepted as a fulfilment of the requirement for the degree of Master of Science (Mechanical Engineering)

.....
Sany Izan Ihsan
Dean, Kulliyyah of Engineering

DECLARATION

I hereby declare that this thesis is the result of my own investigations, except where otherwise stated. I also declare that it has not been previously or concurrently submitted as a whole for any other degrees at IIUM or other institutions.

Aideal Czar Zohary

Signature  Date31/5/2021.....

INTERNATIONAL ISLAMIC UNIVERSITY MALAYSIA

**DECLARATION OF COPYRIGHT AND AFFIRMATION OF
FAIR USE OF UNPUBLISHED RESEARCH**

**EFFECTIVE IMPLEMENTATION OF THE MICROBLOWING
TECHNIQUE ON AIRFOILS**

I declare that the copyright holders of this thesis are jointly owned by the student and IIUM.

Copyright © 2021 Aideal Czar Zohary and International Islamic University Malaysia. All rights reserved.

No part of this unpublished research may be reproduced, stored in a retrieval system, or transmitted, in any form or by any means, electronic, mechanical, photocopying, recording or otherwise without prior written permission of the copyright holder except as provided below

1. Any material contained in or derived from this unpublished research may be used by others in their writing with due acknowledgement.
2. IIUM or its library will have the right to make and transmit copies (print or electronic) for institutional and academic purposes.
3. The IIUM library will have the right to make, store in a retrieved system and supply copies of this unpublished research if requested by other universities and research libraries.

By signing this form, I acknowledged that I have read and understand the IIUM Intellectual Property Right and Commercialization policy.

Affirmed by Aideal Czar Zohary



.....
Signature

.....31/5/2021.....

Date

ACKNOWLEDGEMENTS

In the name Allah, the most beneficent the most merciful,

Show me those who were apart of this quest of knowledge with your continuous blessings
and rahmah.

TABLE OF CONTENTS

| | |
|---|-----------|
| Abstract | ii |
| Abstract in Arabic | iii |
| Approval Page | iv |
| Declaration | vi |
| Copyright Page | vii |
| Acknowledgements..... | viii |
| Table of Contents..... | ix |
| List of Tables..... | xii |
| List of Figures..... | xiii |
| List of Symbols..... | xv |
| List of Abbreviations | xvii |
| | |
| CHAPTER 1: INTRODUCTION | 1 |
| 1.1 Background of the Study..... | 1 |
| 1.2 Statement of the Problem | 2 |
| 1.3 Research Objectives | 3 |
| 1.4 Research Methodology..... | 3 |
| 1.5 Scope of Research..... | 4 |
| 1.6 Thesis Organization | 4 |
| | |
| CHAPTER 2: LITERATURE REVIEW | 5 |
| 2.1 Introduction: UAV Definition and Categories | 5 |
| 2.2 Airfoil Selection for Small/Medium Sized UAV | 6 |
| 2.3 Overview of Drag | 8 |
| 2.4 General Principles Behind Microblowing..... | 11 |
| 2.4.1 Law of the Wall | 12 |
| 2.4.2 Indirect Measurement of Skin Friction Coefficient..... | 16 |
| 2.4.3 Conceptual Design Philosophy..... | 17 |
| 2.5 Development of MBT | 18 |
| 2.6 Recent Works in the Implementation of MBT on Airfoils | 25 |
| 2.7 Chapter Summary | 31 |
| | |
| CHAPTER 3: METHODOLOGY | 33 |
| 3.1 Introduction | 33 |
| 3.2 Part 1: Assessment of 5 Different Airfoils. | 33 |
| 3.2.1 Numerical Algorithm | 35 |
| 3.2.2 Construction of Mesh..... | 38 |
| 3.2.3 Numerical Method | 42 |
| 3.2.4 Mesh Independence Study | 43 |
| 3.2.5 Validation | 46 |
| 3.3 Part 2: CFD Modelling of MBT | 50 |

| | |
|---|------------|
| 3.3.1 Construction of Mesh..... | 50 |
| 3.3.2 Numerical Method | 53 |
| 3.3.3 Boundary Condition..... | 54 |
| 3.3.4 Data Analysis..... | 55 |
| 3.3.5 Mesh Independence Study | 55 |
| 3.3.6 Validation | 56 |
| 3.4 Chapter Summary | 61 |
| CHAPTER 4: RESULTS & DISCUSSION | 63 |
| 4.1 Part 1: Assessment of 5 Different Airfoils | 63 |
| 4.1.1 Drag Decomposition on the Upper Surface | 66 |
| 4.1.2 Drag Decomposition on the Lower Surface..... | 71 |
| 4.1.3 Effect of Variation of Alpha Towards the Critical Point | 74 |
| 4.2 Part 2: Integration of MBT on the S1223 Airfoil | 78 |
| 4.2.1 Revisiting the Literature..... | 78 |
| 4.2.2 Implementation of MBT on the S1223 Airfoil..... | 80 |
| 4.3 CFD Results..... | 82 |
| 4.4 Chapter Summary | 88 |
| CHAPTER 5: CONCLUSION | 89 |
| 5.1 Conclusion..... | 89 |
| 5.2 Recommendation | 90 |
| REFERENCES | 91 |
| APPENDIX I: TABULATED VALIDATION RESULTS | 97 |
| APPENDIX II: PUBLICATION | 100 |

LIST OF TABLES

| | | |
|-----------|--|-------|
| Table 2.1 | The Summary Table on some Categories, Weight, Range and Radius of Flight (Korchenko & Illyash, 2013) | 6 |
| Table 2.2 | Specification of Test Plates (Hwang, 1997) | 19 |
| Table 2.2 | Specification of Test Plates (Hwang, 2002) | 21 |
| Table 3.1 | Mesh quality of the meshes used in this study | 38 |
| Table 3.2 | Effect of Mesh Resolution on c_l | 42 |
| Table 3.3 | Effect of Mesh Resolution on c_d | 42-43 |
| Table 3.4 | Mesh Quality of The Grid Used in this Study | 50 |
| Table 3.5 | Mesh Independence Study for Clark Y and S1223 Airfoil | 53 |
| Table 3.6 | CFD Clark Y Comparison Against XFOIL | 55 |
| Table 3.7 | CFD Clark Y with MBT Comparison Against Experimental Data (Eto, Kondo, Fukagata, & Tokugawa, 2019) | 55 |

LIST OF FIGURES

| | | |
|-------------|--|----|
| Figure 2.1 | Design region of UAV for high and low aspect ratio wing. (Nagel & Shepshelovich, 2004) | 7 |
| Figure 2.2 | Categories of drag (Heyson, Riebe, & Fulton, 1977) | 9 |
| Figure 2.3 | The drag coefficient of a flat plate (Tennekes & Lumley, 2018) | 10 |
| Figure 2.4 | Law of the wall (a) Exaggerated physical depiction (Cengel & Cimbala, 2018) (b) u^+ as a function of y^+ (Tennekes & Lumley, 2018) | 15 |
| Figure 2.5 | Skin friction ratio of GAC 1897 (Hwang, 1997) | 19 |
| Figure 2.6 | Experimental setup and total drag variation as a function of micro blowing rate (Hwang & Biesiadny, 1997) | 20 |
| Figure 2.7 | Setup of the model (Kornilov & Boiko, 2012) | 22 |
| Figure 2.8 | Effect of MBT on the drag and boundary layer base on the law of the wall on a flat perforated plate (Kornilov & Boiko, 2012) | 24 |
| Figure 2.9 | The wing model (Kornilov, 2017) | 25 |
| Figure 2.10 | Variation of the airfoil drag with the angle of attack (Kornilov, 2017) | 26 |
| Figure 2.11 | MBT location on the RAE 2822 airfoil (Gao, Cai, Li, Jiang, & Lee, 2017) | 27 |
| Figure 2.12 | (a) Distributions of the tangential velocity on the first-layer grid for $\alpha = 0^\circ$. (Gao et al., 2017) (b) Numerical results of skin-friction drag ratio (Gao et al., 2017) | 27 |
| Figure 2.13 | Top: Distribution of pressure ratio on the lower wall for Loc6–Loc10 with $\alpha = 0^\circ$ (Gao et al., 2017) | 28 |

Bottom: Numerical results of pressure drag ratio
 ($Ma_\infty = 0.734$, $\alpha = 0^\circ$, and $C_b: 0.008$) (Gao et al., 2017)

| | | |
|-------------|--|-------|
| Figure 2.14 | Schematic of the airfoil (Kornilov, 2018) | 29 |
| Figure 2.15 | Observation at $\alpha = 0^\circ$ (Kornilov, 2018) | 30 |
| Figure 3.1 | Difference between critical momentum thickness Reynolds number, Re_{θ_c} where intermittency starts to grow and transition momentum thickness Reynolds number, Re_{θ_T} where skin friction starts to increase (Langtry, 2006) | 37 |
| Figure 3.2 | S1223 grid (a) Closeup view of the airfoil with guide curves (b) Computational domain | 39 |
| Figure 3.3 | Near airfoil view of the mesh | 40-41 |
| Figure 3.4 | Effect of grid resolution on the skin friction coefficient, c_f on the top surface of the S1223 airfoil at $\alpha: 9.65^\circ$ | 46 |
| Figure 3.5 | Skin friction distribution on the upper surface at corresponding $\alpha(l/d_{max})$ as a function of chord length | 47-48 |
| Figure 3.6 | Coefficient of lift and drag as a function of angle of attack | 48-49 |
| Figure 3.7 | Pressure and skin friction distribution over the lower surface of the FX 61-184 as a function of chordlength at $Re: 1.0 \times 10^6$ (a) $\alpha: 9^\circ$ (b) $\alpha: 10^\circ$ | 49 |
| Figure 3.8 | Pressure and skin friction distribution over the upper surface of the E420 as a function of chordlength at $Re: 1.0 \times 10^6$ (a) $\alpha: 4^\circ$ (b) $\alpha: 6^\circ$ | 50 |
| Figure 3.9 | Constructed mesh, Top: View near the airfoil, Bottom: Guide curves view near the airfoil | 51-52 |
| Figure 3.10 | S1223 MBT Boundary Condition | 55 |
| Figure 3.11 | Structure of the Clark-Y airfoil model (Eto et al., 2019) | 57 |
| Figure 3.12 | CFD comparison on the distribution of the total pressure in the Wake located at $x/c: 1.125$ ($\alpha=0^\circ$) (Eto et al., 2019) | 58 |
| Figure 3.13 | CFD vs Experimental c_f comparison (Eto et al., 2019) | 58 |
| Figure 3.14 | Turbulence intensity profile comparison (Eto et al., 2019) | 60 |

| | | |
|-------------|--|-------|
| Figure 3.15 | Dimensionless boundary layer velocity profile comparison (Eto et al., 2019) | 60 |
| Figure 3.16 | Comparison between the distribution of surface pressure coefficients along the wing chord with a blowing flow rate: 500 l/min at α : 0 and Re : 0.7×10^6 (Kornilov, 2018). | 61 |
| Figure 4.1 | Change in drag composition in terms of percentage of total drag at l/d (max) (Eto et al., 2019) | 64 |
| Figure 4.2 | Drag composition in terms of percentage of total drag as a function of angle of attack. | 64 |
| Figure 4.3 | Aerodynamic performance as a function of angle of attack | 65 |
| Figure 4.4 | Pressure vectors of the upper surface of airfoils along with c_p and c_f distribution as a function of chord length | 66-68 |
| Figure 4.5 | Pressure vectors of the lower surface along with c_p and c_f distribution as a function of chord length | 72-73 |
| Figure 4.6 | Pressure vectors at the angle of attack of zero and l/d (max) along with c_p and c_f distribution as a function of chord length | 75-76 |
| Figure 4.7 | (a) Distribution of surface-pressure coefficients along the wing chord (b) The main structural components of the NACA 0012 wing section | 78 |
| Figure 4.8 | Baseline pressure vector of NACA 0012 | 79 |
| Figure 4.9 | Baseline pressure vector on the lower surface for the S1223 | 81 |
| Figure 4.10 | Effect of MBT with varying blowing fraction | 83 |
| Figure 4.11 | Effect of MBT on aerodynamic performance | 83 |
| Figure 4.12 | Effect of MBT with a blowing fraction of 5% at varying angle of attack | 85-86 |
| Figure 4.13 | Effect of MBT of 5% blowing fraction towards pressure drag as a function of angle of attack | 86 |
| Figure 4.14 | Effect of increasing blowing fraction towards different performance parameters as a function of angle of attack | 87 |

LIST OF SYMBOLS

| | |
|-----------|---|
| c | Chord |
| c_d | Drag coefficient |
| c_f | Skin friction coefficient |
| c_{fo} | Skin friction coefficient for non-porous flat plate |
| c_l | Lift coefficient |
| c_p | Pressure coefficient |
| u | Velocity in x direction |
| u_t | Tangential velocity |
| u_{rms} | Root mean square velocity |
| u_τ | Friction velocity |
| u^+ | Non dimensional tangential velocity |
| y^+ | Non dimensional wall normal direction |
| ν | Kinematic viscosity |
| ρ | Density of material |
| μ | Dynamic viscosity |
| C_b | Blowing coefficient |

LIST OF ABBREVIATIONS

| | |
|----------------|---------------------------------|
| AOA | Angle of Attack |
| CR | Close Range |
| HALE | High Altitude Long Endurance |
| LADP | Low Altitude Deep Penetration |
| LALE | Low Altitude Long Endurance |
| MALE | Medium Altitude Long Endurance |
| MBT | Microblowing Technique |
| MR | Medium Range |
| MRE | Medium Range Endurance |
| RANS | Reynolds-Averaged Navier Stokes |
| RC- Helicopter | Remote Controlled Helicopter |
| Re | Reynolds Number |
| ROA | Remotely Operated Aircraft |
| RPV | Remotely Piloted Vehicle |
| SR | Short Range |
| UAV | Unmanned Aerial Vehicle |
| UCAV | Unmanned Combat Aerial Vehicle |

CHAPTER 1

INTRODUCTION

1.1 BACKGROUND OF THE STUDY

Attempts in controlling the boundary layer can be traced back to about 90 years ago, with increased attention being paid in the 1970s with the goal of decreasing the operational cost for commercial aircrafts (Joslin, 1998). An interesting review on various flow control techniques can be seen in (Gad-el-Hak, 1996). From one perspective, drag reduction can be achieved via suction control that allows the extension of the laminar region on the body. Physically, thinning of the boundary layer promotes stability which then successfully delays transition (Reynolds & Saric, 1986). Since skin friction drag caused by the turbulent boundary layer can be up to 90%, significant research was made to improve the Laminar Flow Control and the Hybrid Laminar Flow Control method through having necessary equipment being installed on the wings, engine nacelles, fuselage nose, as well as the horizontal and vertical tail of an aircraft (Arcara, Bartlett, & McCullers, 1991)

Alternatively, boundary layer control too can be achieved by mass injection or blowing. Aside from flow separation prevention through oscillatory blowing, (Seifert, Bachar, Koss, Shepshelovich, & Wygnanski, 1993; Wang & Sun, 2000) skin friction drag can also be reduced via the Micro Blowing Technique (Hwang, 1997). MBT is superior compared to suction in reducing skin friction drag due to the fact that it executes the objective in a fully developed turbulent flow rather than relying on the extension of laminar zone on the body. Flow instabilities and surface defects in real

application makes it difficult to apply suction techniques and often turbulent boundary layers are needed to prevent flow separation. Further studies also involved MBT to be integrated on engine nacelles (Tillman & Hwang, 1999). Boundary layer flow control via blowing is additionally attractive due to the fact that it has the capability to be implemented passively which will become the ultimate goal.

1.2 STATEMENT OF THE PROBLEM

To establish the scope of this thesis the specific and precise problem statement is outlined below:

Development focusing on fixed-wing Unmanned Aerial Vehicles (UAVs) have been explicitly observed over the past years due to its effective service in numerous fields. Airfoil design optimization, configuration enhancement and propulsion systems modification have yielded continuous accomplishments to date. In addition to that, the integration of the Micro Blowing Technique (MBT) on flat plates which have showed great success in reducing skin friction drag has yet to report sound understanding to lay out the procedures which allow successful total drag reduction when being applied on airfoils. Therefore, there is a need to explore the underlying mechanism to resolve this issue and promote meaningful enhancements in airfoil performance.

For the thesis, research has been done to numerically investigate the effect of implementing MBT on the S1223 airfoil at different angles of attack and Reynolds numbers. The investigation ultimately provides key concepts to allow proper selection of airfoils and blowing placement to ensure MBT to perform well which is absent in the literature. Using the same idea demonstrated in this study, the logic perhaps holds also in the case of suction.

Improved aerodynamic performance translates to reduction in carbon footprints and savings in operational costs. Current enhancements brought by MBT in this study is distinctly significant and is very likely to be further pursued as a passive drag reduction method in future studies.

1.3 RESEARCH OBJECTIVES

This research project has been undertaken to meet the following main objectives:

1. To determine the types of airfoils which are suitable for MBT.
2. To determine the placement constraints of MBT on suitable airfoils.
3. To enhance the aerodynamic performance of a suitable airfoil for low to moderate Re UAV application via introduction of the Micro Blowing Technique.

1.4 RESEARCH METHODOLOGY

This investigation numerically explores the potential of low-speed airfoils being integrated with the Micro Blowing Technique (MBT). The first part of the study consists of assessing the viability of adopting MBT on a selection of airfoils which are suitable for UAV application. Second part follows by modelling MBT on the best candidate airfoil to collect data on the aerodynamic performance improvement brought by this technique.

Preparation of airfoil geometries were done using SOLIDWORKS 2019 while construction of the structured mesh utilizes ICEM CFD and simulations carried using FLUENT from ANSYS 2020 R2 software package. Data on c_l and c_d on the baseline airfoils have all been compared against XFOIL and validated with wind tunnel results.

XFOIL combines a panel method and an integral boundary layer formulation for the analysis of potential and viscous flows around airfoils.

1.5 SCOPE OF RESEARCH

The Reynolds number will be varied from 0.3×10^6 to 1×10^6 and angles of attack ranging from 0-10 degrees. In investigating the relationship between airfoil geometry and profile drag plus selecting candidate airfoil to be implemented with MBT, unsteady transitional modelling will be used to accurately determine the composition of drag of the NACA 4415, FX 61-184, E420, and S1223 airfoil. However, after the candidate airfoil has been selected, further simulation will only be interested in the macroscopic effect of MBT, hence a 2-equation RANS turbulence model will be used.

1.6 THESIS ORGANIZATION

This thesis consists of five chapters. Chapter 1 is the introduction which contains of the overview and background of the study, problem statement, objectives, brief summary of the methodology, and the scope of research. In Chapter 2, relevant information within the scope of the thesis as well as a compilation of the progress in MBT to date are presented followed by highlighting available research gaps in the literature. Then, Chapter 3 focuses on the numerical methodology undertaken to run the simulations that include the procedure in generating the mesh, numerical methods, mesh independence study, boundary conditions, and validation against wind tunnel data. Discussion and assessment of the aerodynamic performance of the S1223 with the integration of MBT are presented in Chapter 4. Finally, in Chapter 5 conclusions are drawn and recommendations are given for further investigations.

CHAPTER 2

LITERATURE REVIEW

2.1 INTRODUCTION: UAV DEFINITION AND CATEGORIES

The name UAV covers all vehicles, which are flying in air with no person on-board with the capability of controlling the aircraft (Eisenbeiss, 2004). The flight of UAVs operates with various degrees of autonomy: either under remote control by a human operator, or fully or intermittently autonomously, by on-board computers. This term is common in the computer science and artificial intelligence community, but terms like Remotely Piloted Vehicle (RPV), Remotely Operated Aircraft (ROA), Remote Controlled Helicopter (RC-Helicopter), and Unmanned Vehicle Systems (UVS) are too often used.

Nowadays there are wide ranges of applications where UAV or drones can be employed. Most of these include military and commercial surveillance, search ,and rescue and most importantly in research purposes (Shakhatreh et al., 2019). Currently, great attention is given to the development of UAVs for improved performance, manoeuvrability, navigation, and stability during operations. The features associated with a UAV may vary depending on its mission so that every given task can be carried out successfully. Classifications of UAV can be done according to the 16 basic features, but this study is primarily inclined towards only one; according to the weight and maximum range of flight (Korchenko & Illyash, 2013). In this category, we can proceed with further grouping as shown in Table 2.1, adapted from (Korchenko & Illyash, 2013) Improvements in the aerodynamic performance of UAVs will promote enhanced

functionality offering greater payload capacity and extension of the maximum range of flight.

Table 2.1
The Summary Table on some Categories of UAVs based on Mass and Maximum Range of Action (Korchenko & Illyash, 2013).

| Category | Subcategory | Mass (kg) | Maximum range of action (km) | |
|---|-------------|--------------|------------------------------|------------|
| | | | with return | w/o return |
| Tactical (Close Range Flights) | Mini | under 20-150 | < 30 | < 60 |
| | CR | 25-150 | 10–30 | 30–80 |
| Operatively–tactical (Short Range Flights) | SR | 50-250 | 30–80 | 90–160 |
| | MR | 150-500 | 80–200 | 240–400 |
| Operative (Medium Range Flights) | MRE | 500-1500 | 200–500 | 600–1000 |
| | LADP | 250-2500 | 250–300 | 700–800 |
| | LALE | 150-250 | 500–800 | 1500–1600 |
| Operatively-strategic (Long Endurance Flights) | MALE | 1000-1500 | 500–800 | 1500–1600 |
| | HALE | 2500-5000 | < 2000 | < 2000 |
| Strategic | | | | |

2.2 AIRFOIL SELECTION FOR SMALL/MEDIUM SIZED UAV

The cost of operation of a UAV can be reduced with airfoil optimization and improvements in the vehicle’s aerodynamic efficiency. Considerations when selecting an airfoil for a UAV include a high maximum lift coefficient, high lift-to-drag ratio, high endurance factor, effectiveness at low Re values, low pitching moment coefficient, mild stall characteristics, insensitivity to surface roughness, good flap performance, and minimal airfoil complexity for ease of manufacturing (Marqués & Ronch, 2017; Nagel & Shepshelovich, 2004; Selig & Guglielmo, 1997). In the presence of high aspect ratio

wings due to configuration development, the optimum endurance performance tends to be inclined towards high loitering lift coefficients with an increase of parasite drag, thus explains the need for a very high lift (Koss, Steinbuch, & Shepshelovich, 1994; Nagel & Shepshelovich, 2004; Selig & Guglielmo, 1997; Steinbuch, Marcus, & Shepshelovich, 2003) as shown in Figure 2.1. The situation is similar for small and medium-size UAVs with their moderate aspect ratio wings.

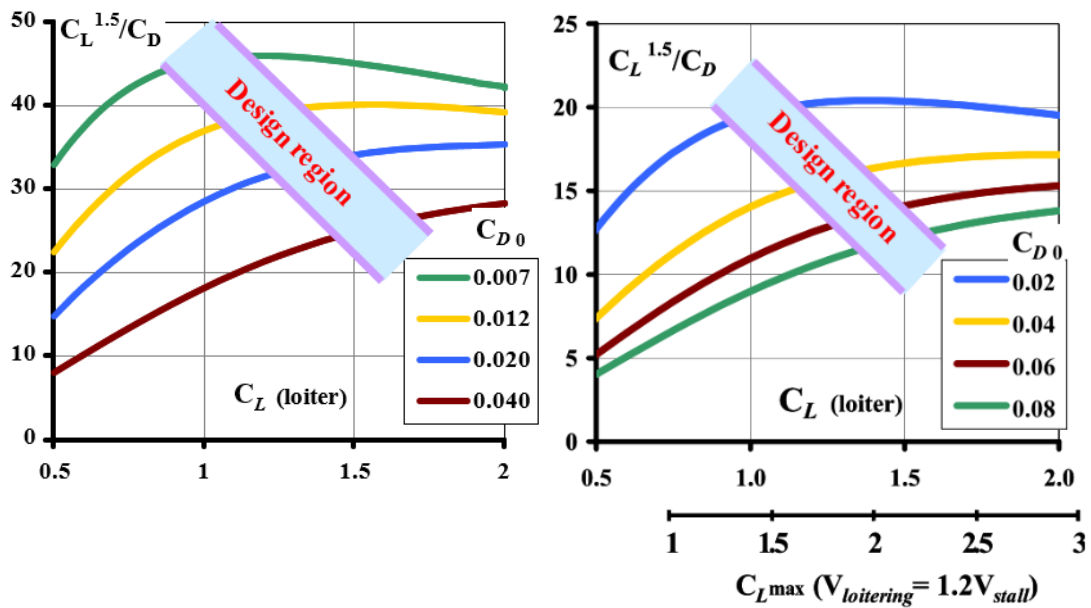


Figure 2.1 Design region of UAV for high and low aspect ratio wings. Left : AR = 25, e = 0.85 Right : AR= 12, e= 0.85 (Nagel & Shepshelovich, 2004)

Apart from that, mild stall characteristics also proved to be important and should be included in the design consideration of small to medium-sized UAVs. This is due to a number of reasons such as reduced sensitivity to contamination effects which leads to safer flights in unfavourable weather conditions. Besides that, the relaxation of the speed safety margin will help in take-off and landing performance where an extended possible variation of flight control can then be accessed. Finally, having compromised

speed safety margins will also allow the aircraft to fly at a higher lift coefficient and result in improved endurance.

Over the years, a wealth of airfoils have been uniquely tailored to deliver optimal performance for their intended mission. The NACA 4415 for instance not only serves the American unmanned aerial vehicle such as the AAI Shadow 200 and AAI RQ-2 Pioneer, but also have been seen included in the design for wind and hydrokinetic turbine application (Bertagnolio, Sørensen, Johansen, & Fuglsang, 2001; Mohammadi, Hassanalian, Arionfard, & Bakhtiyarov, 2020; Ozgener, 2006). The Akaflieg Darmstadt D-38,39 and 39b German sailplanes (Lednicer, 2010) on the other hand adopted the classical FX 61-184 by Wortmann (Althaus & Wortmann, 1981) which features a concave-type of pressure recovery to reduce the severity of increased drag with increasing angle of attack. Some years later, improved high lift airfoils were designed based on this concept and highlights include the E420 airfoil (Eppler, 2012) which is recommended for operations that exceed a Reynolds number of one million and the S1223 preferred for smaller UAVs (Selig, 1995). Since small to medium-sized UAVs typically operate between a Reynolds number of 3×10^4 to 2×10^6 , (Marqués & Ronch, 2017; Selig & Guglielmo, 1997; Windte, Radespiel, Scholz, & Eisfeld, 2004) these airfoils have great potential to be further improved with drag reduction techniques.

2.3 OVERVIEW OF DRAG

Aerodynamic drag in incompressible flows generally consists of profile drag and induced drag as shown in Figure 2.2. Viscous effects give rise to the concept of the boundary layer, where it is simply defined as a region where the flow near a body is retarded due to the no-slip condition. The development of the boundary layer depends on a range of parameters which include the pressure gradient, freestream turbulence,

surface roughness, flow instabilities, and Reynolds number (Anderson Jr, 2010). From the perspective of ensuring continuous attached flow on a body, turbulent boundary layers with higher energy levels are preferred since it is less susceptible to experience separation in adverse pressure gradient flows. This allows airfoils to operate at a higher angle of attack and achieve greater production of lift. However, drawback comes in the form that the turbulent boundary layer generates a considerable amount of wall shear stress unto the body as shown in Figure 2.3.

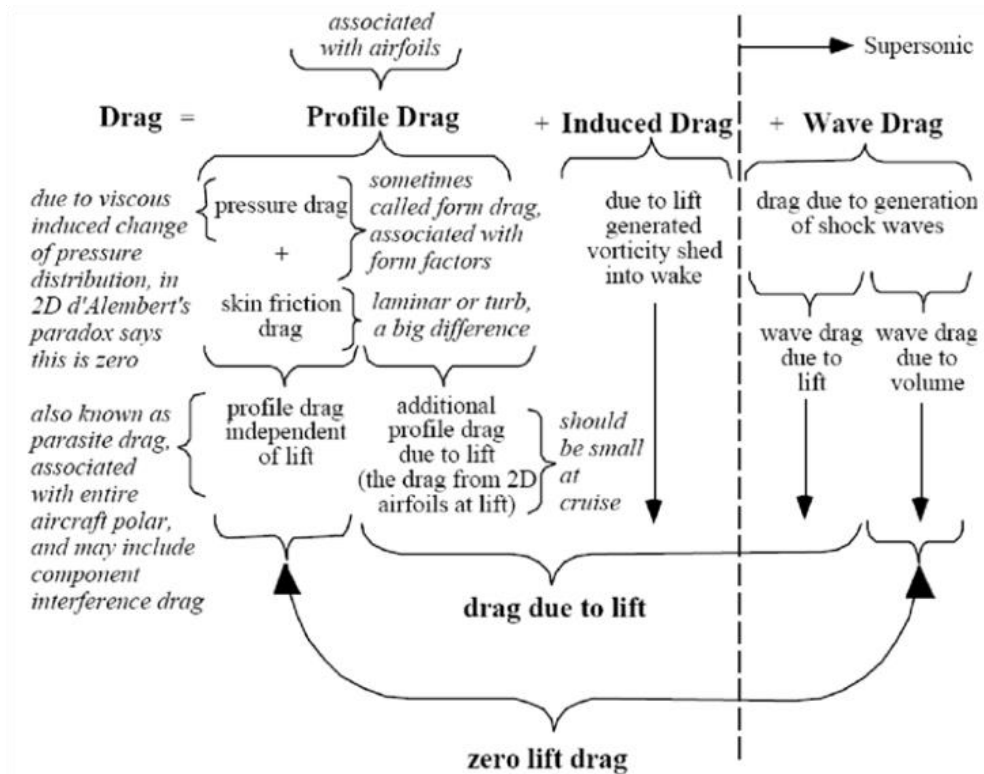


Figure 2.2 Categories of drag (Heyson et al., 1977)

Within the operating conditions of an airfoil, the degree of acceleration of the flow along its body imposes the suction effect to be felt on the upper surface, and vice versa on the lower surface. Since pressure forces always act in the direction normal to the curvature of the body, the integration of this force along the surface will have